Journal of Materials Chemistry A

Accepted Manuscript

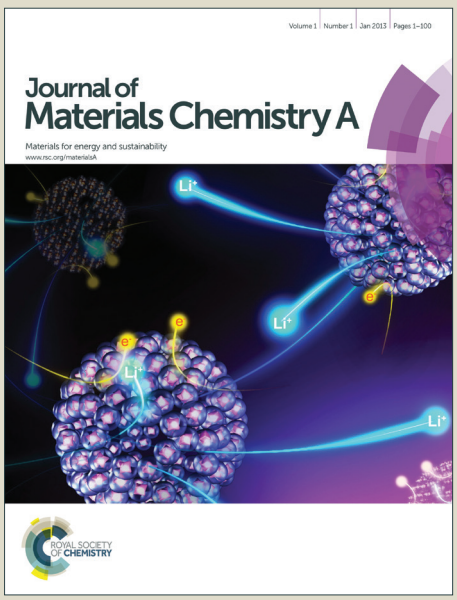

ROYAL SOCIETY OF CHEMISTRY

www.rsc.org/materialsA

Table of Contents Entry

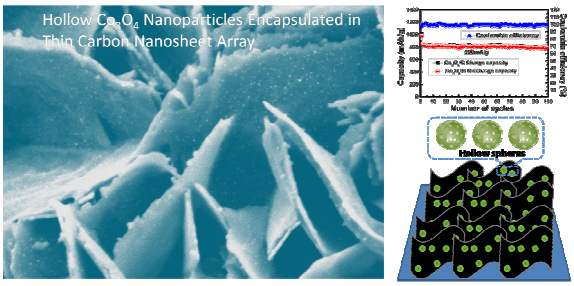

A facile method is introduced to synthesize hollow Co_3O_4-NPs encapsulated in thin carbon nanosheets array as anode materials in LIBs.

Designed Synthesis of Hollow Co_3O_4 Nanoparticles Encapsulated in Thin Carbon Nanosheet Array for High and Reversible Lithium Storage

Liang Peng, Yangyang Feng, Yuanjuan Bai, Hua-Jun Qiu, Yu Wang**

The State Key Laboratory of Mechanical Transmissions and School of Chemistry and Chemical Engineering, Chongqing University, Chongqing 400044, China

*Email: wangy@cqu.edu.cn (Y.W.);

hjqiu@cqu.edu.cn (H.J.Q.)

Abstract

The design and fabrication of novel composite nano-architecture is crucial for their applications in energy storage devices such as lithium ion batteries (LIBs). Herein, a thin carbon nanosheet array with encapsulated hollow Co_3O_4 nanoparticles is successfully fabricated on 3D Ni foam by using the electrodeposited $Co(OH)_2$ nanosheets as templates and followed by two step annealing process. When used as an anode material in LIBs, the hollow Co_3O_4/carbon nanosheets composite displays an excellent performance with a high reversible capacity, excellent cycling stability and rate capability. This work is helpful for the design of advanced electrode for LIBs, supercapacitors, electrochemical sensors, etc.

Keywords: nanosheet array, binder-free electrode, Co_3O_4, lithium ion batteries

Introduction

The growing energy consumption and global warming call for urgent development of clean energy technology.[1-4] As a green power source, lithium ion batteries (LIBs) have been widely used in modern society and also attracted great research interest due to the importance.[5-8] So far, various materials such as graphitic/non-graphitic carbon, transition metal oxides and their composites, etc., have been exploited as the anode materials for LIBs.[9-11] Among them, the transition metal oxides such as Co_3O_4 attract

a lot research interest as an anode material due to its high theoretical capacity (890 mAh g^{-1}).[12-17] However, the large volume expansion/contraction and severe particle aggregation during the Li insertion/extraction process would lead to electrode pulverization and loss of interparticle contact, resulting in a large irreversible capacity loss and poor cycling stability.[18, 19] To solve these problems, different strategies have been tried, including the fabrication of carbon-based nanocomposites, low dimensional Co_3O_4 nanostructures, hollow structure, etc.[12, 18, 20, 21] Among these, the fabrication of composites with different carbon nanomaterials has been proved to be very promising.[22-24] However, the carbon-based composites are commonly prepared by simply depositing active materials on carbon surfaces.[25-28] Due to the one-side attachment, the active material such as Co_3O_4 may be easily peeled off from the carbon surfaces during continuous charge-discharge reactions. To enhance the structure stability, the encapsulation of active nanomaterials inside two closely attached thin carbon nanosheets should be a better strategy.[29, 30] However, the design and fabrication of closely encapsulated cobalt oxide-based composite electrodes remains a big challenge.

It is known that the electrodes for electrochemical LIBs test are usually binder-rich ones prepared by the traditional slurry coating technique which may make some electroactive materials blocked from the electrolyte. Moreover, the polymer binder will decrease the electronic conductivity of the electrode materials, hence lowering their electrochemical performance.[31] Based on these considerations, the design and fabrication of 3D binder-free electrode with strongly attached 1D or 2D nanostructure array should enhance the kinetics of ion and electron transport in electrodes and the structure stability of the electrode materials during Li insertion/extraction process, resulting in an enhanced performance of LIBs.[32, 33]

In this study, using electrodeposited $Co(OH)_2$ nanosheet array as templates, we design and fabricate a thin carbon nanosheet array on Ni foam with hollow Co_3O_4 nanoparticles (NPs) encapsulated inside of the carbon nanosheets. Due to the unique structure design and enhanced material properties, the binder-free hollow Co_3O_4 NPs/carbon nanosheet array electrode exhibits a large reversible capacity with an excellent cycling stability and high rate capability when used as a free-standing anode material for LIBs.

Experimental Section

Materials: All materials or chemicals are of analytical grade and used as received. $Co(NO_3)_2 \cdot 6H_2O$ (99.9%), metallic Li foil (99.9%) and D(+)-glucose are obtained from Aldrich. Nickel foam is from Alfa Aesar.

Synthesis of $Co(OH)_2$ nanosheet array on Ni foam.

Prior to the synthesis, Ni foam (1 cm × 2 cm) was rinsed with concentrated HCl solution (37 wt%) in an ultrasound bath for 10 min to remove the surface NiO layer. The electrodeposition was performed in a standard three-electrode cell consisting of the clean Ni foam working electrode, a platinum plate counter electrode and a saturated calomel reference electrode (SCE) at room temperature. The $Co(OH)_2$ nanosheet array was electrodeposited on Ni foam substrate in a 0.05 M $Co(NO_3)_2 \cdot 6H_2O$ aqueous electrolyte using an CHI 660E electrochemical workstation at a constant potential of -1.0 V (vs. SCE) for 20 min. After that, the $Co(OH)_2$/Ni foam was carefully rinsed several times with deionized water and ethanol, and then dried in air.

Synthesis of Co_3O_4/carbon nanosheet array on Ni foam.

The $Co(OH)_2$/Ni foam (1 cm × 2 cm) was ultrasonically mixed with 5 mL glucose aqueous solution (1 M) and 35 mL water for 15 min. The above mixture was transferred into a 50 mL Teflon-lined autoclave, sealed tightly and heated in an electric oven at 180 ^oC for 4 h. When the sample was cooled to room temperature, it was taken out and washed with water and ethanol. After that, the sample was dried in an oven at 60 ^oC overnight to remove the residue water and ethanol. After coated with polymerized glucose molecules on the $Co(OH)_2$ nanosheet surface, the sample was annealed at 700 ^oC for 200 min in H_2 atmosphere to form the Co/carbon nanosheet array which was then calcined in air at 250 ^oC for 2 h with a ramping rate of 1 ^oC/min to form the hollow Co_3O_4 nanoparticles encapsulated in the thin carbon nanosheet array (Co_3O_4/carbon nanosheets). In average, about 1.8 mg of Co_3O_4/carbon nanosheets was grown on the 1 cm^2 Ni foam, which was calculated based on the mass difference before and after the fabrication.

Carbon content tests

To precisely calculate the battery performance, we also fabricated the composite on flat Ni sheet surface so that these composite can be easily scraped off by a thin knife. The Co_3O_4/carbon composite (200 mg) were mixed with concentrated HCl solution for 24 h to completely dissolve the Co_3O_4 NPs. The carbon remain was collected, carefully rinsed and dried in an oven at 60 ^oC overnight. The carbon weight was measured by using a Mettler-Toledo analytical balance. The concentration of carbon in the composite was around 8.5%.

Material Characterizations.

The fabricated materials were characterized by powder X-ray diffraction (Bruker D8 Advance X-ray diffractometer) with Cu Kα radiation, scanning electron microscope (SEM, JEOL, JSM-7800F) with an energy dispersive spectrometer (EDS), transmission electron microscopy (TEM, JEOL, JEM-2100F), Brunauer-Emmett-Teller surface-area and pore-size analyzer (BET, Quantachrome Autosorb-6B) and Raman spectroscopy (RENISHAW Invia Raman Microscope, voltage (AC) 100-240 V, power 150 W).

Electrochemical Measurements

Prior to the battery test, the Ni foam loaded with Co_3O_4/carbon nanosheet was cut into smaller pieces (1 cm × 1 cm) and used as binder-free working electrodes. A lithium metal was used as the counter and reference electrode and a Celgard 2400 membrane was used as the cell separator. The electrolyte was 1 M $LiPF_6$ in ethylene carbonate and diethyl carbonate (EC-DEC, v/v=1:1). The cells were constructed in an Ar-filled glove box. The galvanostatic cycling was performed on Neware battery testing system, and cyclic voltammetry (CV) was collected using Autolab (model of AUT71740). The electrochemical impedance measurements were carried out by applying an AC voltage of 5 mV in the frequency from 0.01 Hz to 100 kHz. The specific capacity and current density were calculated based on the mass of the active material in the working electrode.

Results and discussion

Preparation and characterization of hollow Co_3O_4/carbon nanosheet array on Ni foam

The fabrication process of the hollow Co_3O_4 nanoparticles encapsulated in thin carbon nanosheet arrays is shown in Scheme 1a. First, pure $Co(OH)_2$ nanosheets were grown on Ni foam by a electrodeposition method.[34, 35] Based on the rich –OH group on the nanosheet surface, a second step hydrothermal process was then carried out to prepare the carbonized glucose layers using glucose as a green carbon source. The carbonized glucose-coated $Co(OH)_2$ nanosheets were then annealed in H_2 atmosphere at 700 °C. This annealing process would crystalize the carbonized glucose layers into graphitic thin carbon nanosheet arrays which inherit the morphology of the $Co(OH)_2$ nanosheets. At the same time, the $Co(OH)_2$ nanosheets are decomposed (reduced) into pure Co nanoparticles encapsulated inside of the thin carbon nanosheeet array. Finally, a second annealing in air was carried out to transform the Co NPs/carbon nanosheets into hollow Co_3O_4 NPs/carbon nanosheet array on Ni foam. As shown in Scheme 1b, the mechanism for the formation of hollow Co_3O_4 NPs from Co NPs is due to the nanoscale Kirkendall effect which has also been observed by annealing Ni or Cu NPs in different atmospheres.[36]

Fig. 1a shows the SEM image of the electrodeposited $Co(OH)_2$ nanosheet array on Ni foam. It is observed that the thin nanosheets are uniformly distributed on the Ni foam ligament surface and exhibit an average size of around 2 micrometers from the section view (Fig. 1b). From the zoom-in SEM image (Fig. 1c), it is observed that the thin $Co(OH)_2$ nanosheet is several tens nanometers in thickness. The nanosheets are interconnected forming a porous network structure. After the electrodeposition, the Ni foam exhibits a clear color change from light gray to green (Fig. 1d). XRD analysis (Figure S1 in supporting information) shows that the formed nanosheets are pure α-$Co(OH)_2$.[34, 37] After the carbonized glucose coating and two-step annealing, the morphology of the $Co(OH)_2$ nanosheets is well-inherited by the formed carbon nanosheet array (Fig. 2a and 2b). The formed Co_3O_4 NPs with a size of ~10-20 nm are uniformly distributed inside of the thin carbon nanosheets from the high magnification image (Fig. 2c and 2d). Also, the coating and annealing treatments turn the color of the modified Ni foam into black from green (Fig. 1d).

The encapsulated Co_3O_4 NPs are further characterized by TEM. As shown in Fig. 3a, high density and uniform Co_3O_4 NPs with diameter of ~10-20 nm are homogeneously encapsulated inside of the thin carbon nanosheets, which is in good agreement with the SEM result. The zoom-in TEM image shows a clear color contrast between the hollow core and surface shell, indicating that the Co_3O_4 NPs have a hollow structure (Fig. 3b). The continuous lattice fringes in the HRTEM image (Fig. 3c) indicate the crystalline nature of the encapsulated Co_3O_4 NPs. The lattice spacing of 0.24 nm corresponds to the (311) plane of Co_3O_4. The crystal structure of the Co_3O_4/carbon nanosheet array is further characterized by XRD (Fig. 3d). The three strong diffraction peaks at 45.5°, 53.0°, and 78.3° can be ascribed to the Ni foam substrate. The relatively weak diffraction peaks at the degree of 19° (111), 31.2° (220), 36.8° (311), 59.3° (511) and 65.2° (440) are consistent with the standard XRD data for Co_3O_4 (JCPDS No. 43-1003). EDS analysis further shows that carbon, oxygen, and cobalt are the main elements of the composite (Fig. S2). The signal of Si is from the substrate used for the EDS test.

The graphitization degree of the thin carbon nanosheets is characterized by Raman spectroscopy. It is known that the D band peak indicates the disordered graphitic crystal stacking while G band increases with the number of the graphene layers.[30, 38, 39] The degree of crystallization of the carbon sheets can be relatively determined by the I_D/I_G ratio. A lower I_D/I_G ratio corresponds to a high crystallization degree. As shown in Fig. 4a, the I_D/I_G ratio of the carbon nanosheet is less than 1, which is similar to that of reduced graphene oxides, indicating the good crystallization by the first step annealing at the high temperature. The Brunauer–Emmett–Teller (BET) surface area of the composite is determined to be ~243 $m^2 g^{-1}$ and pore diameter is around 3.6 nm with the Barrett-Joyner-Hallender (BJH) method (Fig. 4b and 4c). These results suggest that the carbon nanosheets possess a high surface area and many small pores which would facilitate the free diffusion of electrolyte during electrochemical reactions.

Electrochemical measurement

The binder-free carbon nanosheet array network with encapsulated hollow Co_3O_4 NPs should be a promising anode material for LIBs. Fig. 5a shows the galvanostatic discharge-charge curves of the Co_3O_4/carbon nanosheets at 0.1 A g^{-1} between 0.01 and 3.0 V *vs* Li/Li^+. It is observed that the Co_3O_4/carbon nanosheet array exhibits a high initial discharge capacity of ~1780 mAh g^{-1}, which is significantly higher than the theoretical capacity of Co_3O_4 (890 mAh g^{-1}). The excess discharge capacity could be associated with the initial formation of the solid-electrolyte-interface (SEI) layer resulted from electrolyte degradation, which is a common phenomenon and also observed in many other anode materials.[42-44] From the second cycle, the capacity decreases to ~1081 mAh g^{-1} and the charge-discharge process becomes much stable (Fig. 5a). After even 100 cycles at 0.5 A g^{-1}, the capacity retained is still over 97% with high Coulombic efficiency (~98%), indicating the excellent cycling stability of the Co_3O_4/carbon nanosheet composite (Fig. 5b). As observed from the SEM image in Fig. S3, after the 100 charge-discharge cycles, the structure integrity of the binder-free 3D array electrode is still well retained. The stabilized specific capacity (~1052 mAh g^{-1} at 0.1 A g^{-1}) is also remarkably high when compared with most reported values of Co_3O_4-based anode materials such as Co_3O_4 octahedral nanocages (887 mAh g^{-1} at 0.2 C),[24] Co_3O_4/graphene composite (754 mAh g^{-1} at 0.1 A g^{-1})[43] and carbon-coated Co_3O_4 nanotubes (823 mAh g^{-1} at 0.2 A g^{-1}).[24, 45, 46] More comparisons have been listed in Supporting Information (Table S1). Based on recent studies,[40, 41] Co_3O_4 shows the Li-storage activity for LIBs through reduction/oxidation reaction. In the first discharging process, Co_3O_4 is reduced to Co through an eight electron reaction process: $Co_3O_4 + 8Li^+ \rightarrow 3Co + 4Li_2O$. Subsequently, the charge and discharge process is reversible through a two electron reaction process: $Co + Li_2O \leftrightarrow CoO + 2Li^+ + 2e^-$. Thus, the electron number difference between the two reaction processes should also contribute the large capacity difference between the first discharge process and the subsequent charge/discharge process.

To test the rate performance, continuous increase in current density from 0.1 A g^{-1} to 10 A g^{-1} was carried out (Fig. 5c). It is observed that the capacity decreases with the increase of current densities (Fig. 5d). When 10 A g^{-1} is applied, the capacity is still ~463 mAh g^{-1} (~52%), which also higher than those of previous reports,[45, 47] indicating the good rate capability of the binder-free array electrode. Moreover, when

cycled back to 0.1 A g^{-1}, the recovered capacity can reach ~1052 mAh g^{-1}, which further demonstrates the excellent performance of the designed binder-free composite electrode. The high and stable Li storage performance is clearly resulted from the designed unique structure of the anode. Firstly, the porous carbon nanosheet network can remarkably enhance the electronic conductivity and the diffusion of electrolyte and ions.[25, 48, 49] As shown in impedance spectrum in Fig. S4, the carbon nanosheet-based composite exhibits a very low charge-transfer resistance. Due to the direct attachment to the Ni foam current collector, the aggregation and stacking between individual carbon sheets in normal electrode are completely avoided.[50, 51] A schematic explanation about the working mechanism of the array electrode is presented in Fig. S5. Secondly, due to the encapsulation in the carbon nanosheets, the detachment, aggregation, and even pulverization of the hollow Co_3O_4 NPs can be largely solved.[30, 52] Thirdly, the efficient inner space from the hollow core would allow the volume expansion of the Co_3O_4 shells while retaining the structure integrity. [40, 50] Finally, the nanoscale hollow Co_3O_4 particles (~10-20 nm) with high surface areas will effectively improve the Li-ion exchange rate.

Conclusions

A uniformly distributed carbon nanosheet array with encapsulated hollow Co_3O_4 NPs was easily prepared by using electrodeposited $Co(OH)_2$ nanosheets as templates, and followed by surface glucose polymerization and two-step annealing process. This designed binder-free 3D composite electrode possesses many unique structure properties such as intimate contact between the encapsulated hollow nanoparticles and thin carbon nanosheets, high nanoporosity, large specific surface area, etc. Owing to the unique nano-architecture, the Co_3O_4/carbon nanosheets array exhibits a high and stable performance when used as anode materials in LIBs. We believe that this work presents a new strategy on designing advanced carbon-encapsulated binder-free nanocomposite electrode for various electrochemical applications.

Acknowledgements

Financial support is from Thousand Young Talents Program of the Chinese Central Government (No. 0220002102003), National Natural Science Foundation of China

(NSFC, No. 21373280, 21403019), Beijing National Laboratory for Molecular Sciences (BNLMS) and Hundred Talents Program at Chongqing University (No. 0903005203205).

Reference

1. N. Oyama, T. Tatsuma, T. Sato and T. Sotomura, *Nature*, 1995, **373**, 598-600.
2. J. Chmiola, C. Largeot, P. L. Taberna, P. Simon and Y. Gogotsi, *Science*, 2010, **328**, 480-483.
3. H. Sun, X. You, J. E. Deng, X. L. Chen, Z. B. Yang, J. Ren and H. S. Peng, *Adv. Mater.*, 2014, **26**, 2868-2873.
4. R. Costi, A. E. Saunders, E. Elmalem, A. Salant and U. Banin, *Nano Lett.*, 2008, **8**, 637-641.
5. M. Armand and J. M. Tarascon, *Nature*, 2008, **451**, 652-657.
6. S. Y. Liu, J. Xie, Q. M. Su, G. H. Du, S. C. Zhang, G. S. Cao, T. J. Zhu and X. B. Zhao, *Nano Energy*, 2014, **8**, 84-94.
7. J. Liu, K. P. Song, P. A. van Aken, J. Maier and Y. Yu, *Nano Lett.*, 2014, **14**, 2597-2603.
8. C. J. Niu, J. S. Meng, C. H. Han, K. N. Zhao, M. Y. Yan and L. Q. Mai, *Nano Lett.*, 2014, **14**, 2873-2878.
9. Y. Yamauchi, A. Tonegawa, M. Komatsu, H. Wang, L. Wang, Y. Nemoto, N. Suzuki and K. Kuroda, *J. Am. Chem. Soc.*, 2012, **134**, 5100-5109.
10. D. H. Wang, D. W. Choi, J. Li, Z. G. Yang, Z. M. Nie, R. Kou, D. H. Hu, C. M. Wang, L. V. Saraf, J. G. Zhang, I. A. Aksay and J. Liu, *ACS Nano*, 2009, **3**, 907-914.
11. J. S. Chen, H. Liu, S. Z. Qiao and X. W. Lou, *J. Mater. Chem.*, 2011, **21**, 5687-5692.
12. H.-J. Qiu, L. Liu, Y.-P. Mu, H.-J. Zhang and Y. Wang, *Nano Res.*, 2014, 1-19.
13. M. V. Reddy, G. V. Subba Rao and B. V. R. Chowdari, *Chem. Rev.*, 2013, **113**, 5364-5457.
14. C. Peng, B. Chen, Y. Qin, S. Yang, C. Li, Y. Zuo, S. Liu and J. Yang, *ACS Nano*, 2012, **6**, 1074-1081.
15. Y. Sun, X. Hu, W. Luo and Y. Huang, *J. Phys. Chem. C*, 2012, **116**, 20794-20799.
16. K. Xie, P. Wu, Y. Zhou, Y. Ye, H. Wang, Y. Tang, Y. Zhou and T. Lu, *ACS Appl. Mater. Interfaces*, 2014, **6**, 10602-10607.
17. C. Zhou, Y. Zhang, Y. Li and J. Liu, *Nano Lett.*, 2013, **13**, 2078-2085.
18. Z. S. Wu, W. C. Ren, L. Wen, L. B. Gao, J. P. Zhao, Z. P. Chen, G. M. Zhou, F. Li and H. M. Cheng, *ACS Nano*, 2010, **4**, 3187-3194.
19. H. Wu, M. Xu, Y. C. Wang and G. F. Zheng, *Nano Res.*, 2013, **6**, 167-173.
20. Y. Wang, H. J. Zhang, L. Lu, L. P. Stubbs, C. C. Wong and J. Y. Lin, *ACS Nano*, 2010, **4**, 4753-4761.
21. H. J. Liu, S. H. Bo, W. J. Cui, F. Li, C. X. Wang and Y. Y. Xia, *Electrochim. Acta*, 2008, **53**, 6497-6503.
22. J. Zhi, S. Deng, Y. Zhang, Y. Wang and A. Hu, *J. Mater. Chem. A*, 2013, **1**, 3171-3176.
23. F. Zhang, T. Zhang, X. Yang, L. Zhang, K. Leng, Y. Huang and Y. Chen, *Energy Environ. Sci.*, 2013, **6**, 1623-1632.
24. L. Zhuo, Y. Wu, J. Ming, L. Wang, Y. Yu, X. Zhang and F. Zhao, *J. Mater. Chem. A*, 2013, **1**, 1141-1147.
25. Y. Lu, X. Wang, Y. Mai, J. Xiang, H. Zhang, L. Li, C. Gu, J. Tu and S. X. Mao, *J. Phys. Chem. C*, 2012, **116**, 22217-22225.
26. G. Zhou, D.-W. Wang, F. Li, L. Zhang, N. Li, Z.-S. Wu, L. Wen, G. Q. Lu and H.-M. Cheng, *Chem. Mater.*, 2010, **22**, 5306-5313.

27. S. Yang, X. Feng, S. Ivanovici and K. Müllen, *Angew. Chem. Int. Ed.*, 2010, **49**, 8408-8411.
28. S.-W. Kim, D.-H. Seo, H. Gwon, J. Kim and K. Kang, *Adv. Mater.*, 2010, **22**, 5260-5264.
29. Y. Wang, Y. Bai, X. Li, Y. Feng and H. Zhang, *Chem. Eur. J.*, 2013, **19**, 3340-3347.
30. H. Zhang, Y. Bai, Y. Feng, X. Li and Y. Wang, *Nanoscale*, 2013, **5**, 2243-2248.
31. Y. G. Li, B. Tan and Y. Y. Wu, *Nano Lett.*, 2008, **8**, 265-270.
32. J. Liu, K. Song, P. A. van Aken, J. Maier and Y. Yu, *Nano Lett.*, 2014, **14**, 2597-2603.
33. X. Wang, L. Qiao, X. Sun, X. Li, D. Hu, Q. Zhang and D. He, *J. Mater. Chem. A*, 2013, **1**, 4173-4176.
34. C. Yuan, L. Yang, L. Hou, L. Shen, X. Zhang and X. W. Lou, *Energy Environ. Sci.*, 2012, **5**, 7883-7887.
35. J. Du, G. Zhou, H. Zhang, C. Cheng, J. Ma, W. Wei, L. Chen and T. Wang, *ACS Appl. Mater. Interfaces*, 2013, **5**, 7405-7409.
36. J. G. Railsback, A. C. Johnston-Peck, J. Wang and J. B. Tracy, *ACS Nano*, 2010, **4**, 1913-1920.
37. J. Yang, H. Liu, W. N. Martens and R. L. Frost, *The J. Phys. Chem. C*, 2009, **114**, 111-119.
38. J. Ha, S. K. Park, S. H. Yu, A. Jin, B. Jang, S. Bong, I. Kim, Y. E. Sung and Y. Piao, *Nanoscale*, 2013, **5**, 8647-8655.
39. E. Flahaut, F. Agnoli, J. Sloan, C. O'Connor and M. L. H. Green, *Chem. Mater.*, 2002, **14**, 2553-2558.
40. J. Chen, X.-h. Xia, J.-p. Tu, Q.-q. Xiong, Y.-X. Yu, X.-l. Wang and C.-d. Gu, *J. Mater. Chem.*, 2012, **22**, 15056-15061.
41. Q. M. Su, J. Zhang, Y. S. Wu and G. H. Du, *Nano Energy*, 2014, **9**, 264-272.
42. L. Zhang, H. B. Wu and X. Wen Lou, *Mater. Horiz.*, 2014, **1**, 133-138.
43. H. Zhong, G. Yang, H. Song, Q. Liao, H. Cui, P. Shen and C.-X. Wang, *J. Phys. Chem. C*, 2012, **116**, 9319-9326.
44. B. Wang, J. S. Chen, H. B. Wu, Z. Wang and X. W. Lou, *J. Am. Chem. Soc.*, 2011, **133**, 17146-17148.
45. D. Liu, X. Wang, W. Tian, Y. Bando and D. Golberg, *Sci. Rep.*, 2013, **3**, 2543.
46. S. Yang, G. Cui, S. Pang, Q. Cao, U. Kolb, X. Feng, J. Maier and K. Mullen, *Chemsuschem*, 2010, **3**, 236-239.
47. A. Q. Pan, Y. P. Wang, W. Xu, Z. W. Nie, S. Q. Liang, Z. M. Nie, C. M. Wang, G. Z. Cao and J. G. Zhang, *J. Power Sources*, 2014, **255**, 125-129.
48. H. J. Zhang, Y. Y. Feng, Y. Zhang, L. Fang, W. X. Li, Q. Liu, K. Wu and Y. Wang, *Chemsuschem*, 2014, **7**, 2000-2006.
49. Z. C. Xing, A. M. Asiri, A. Y. Obaid, X. P. Sun and X. Ge, *Rsc Adv.*, 2014, **4**, 9061-9063.
50. H. J. Zhang, Y. J. Bai, Y. Zhang, X. Li, Y. Y. Feng, Q. Liu, K. Wu and Y. Wang, *Sci. Rep-Uk*, 2013, **3**.
51. J. C. Liu, Y. J. Xu, X. J. Ma, J. K. Feng, Y. T. Qian and S. L. Xiong, *Nano Energy*, 2014, **7**, 52-62.
52. B. Wang, Y. Wen, D. Ye, H. Yu, B. Sun, G. Wang, D. Hulicova-Jurcakova and L. Wang, *Chemistry*, 2014, **20**, 5224-5230.

Figure captions:

Scheme 1. (a) Schematic illustration of the designed electrode fabrication process. (b) Schematic illustration of the formation of Co_3O_4 hollow NPs.

Fig. 1. SEM images of α-$Co(OH)_2$ nanosheet arrays (a: low magnification; b: section view; c: high magnification) and photos of the nanosheet array before and carbon coating/annealing. Inset in (a) shows the SEM image of the Ni foam substrate.

Fig. 2. SEM images of the Co_3O_4/carbon nanosheet array with different magnifications.

Fig. 3. TEM (a: low magnification; b: high magnification) and HRTEM (c) images of the Co_3O_4/carbon nanosheet array. XRD pattern of the nanocomposite (d) with the standard pattern of Co_3O_4 attached for comparison.

Fig. 4. Nitrogen absorption/desorption curve (a), pore size distribution (b) and Raman spectrum (c) of the Co_3O_4/carbon nanosheets.

Fig. 5. Galvanostatic charge-discharge curves of the electrode at different cycles at 0.1 A g^{-1} (a). Cycling performance and coulombic efficiency of the Co_3O_4/carbon nanosheet array at a current density of 0.5 A g^{-1} (b). Galvanostatic charge-discharge curves (c) of the Co_3O_4/carbon nanosheet array at different current densities and the rate capability test (d).

Scheme 1

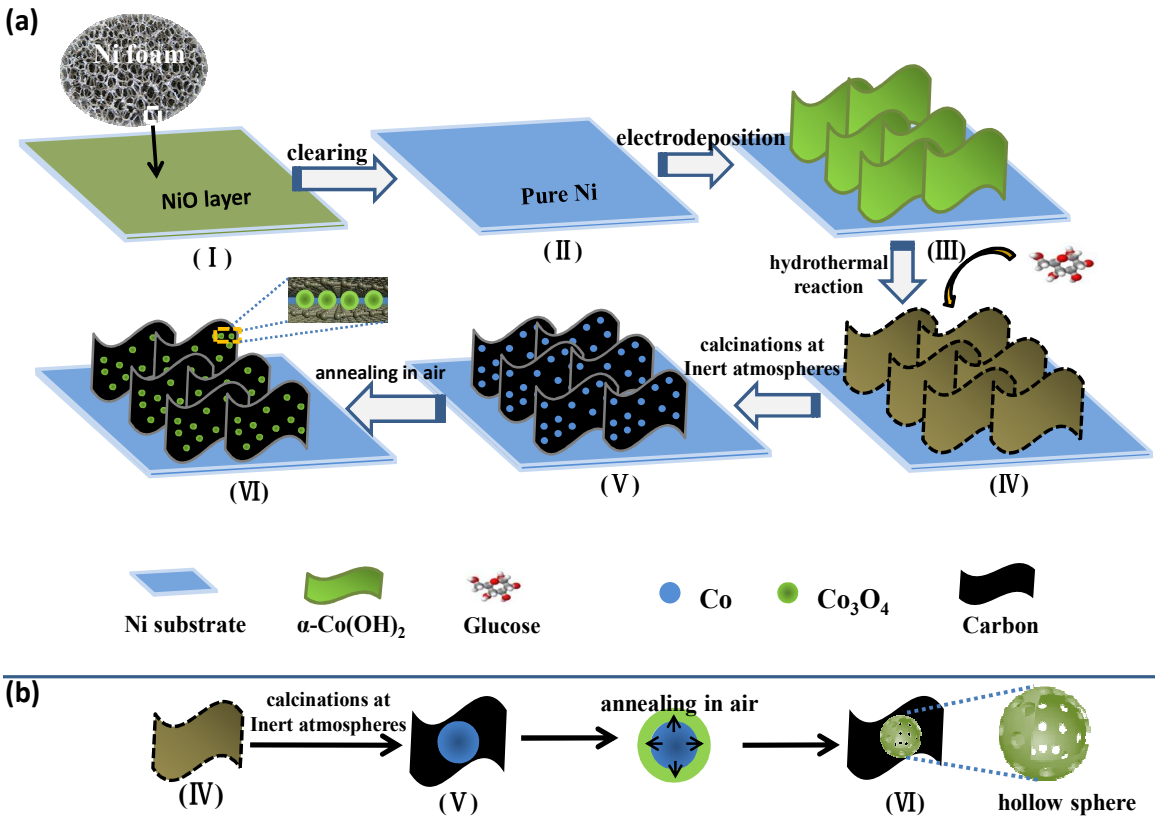

Fig. 1

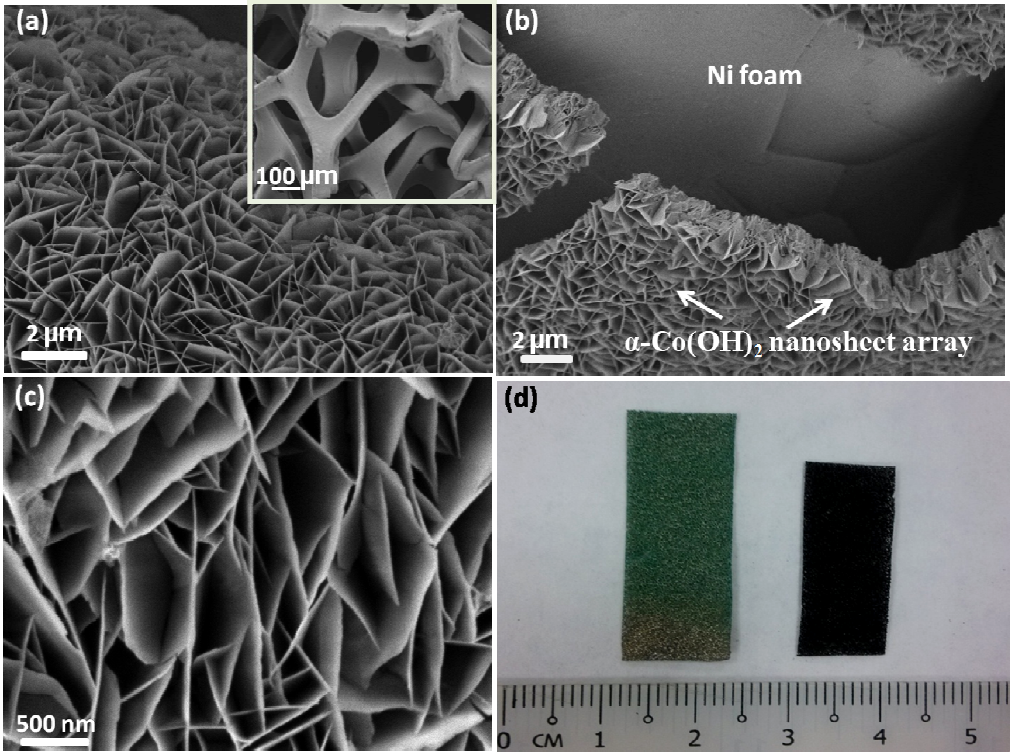

Fig. 2

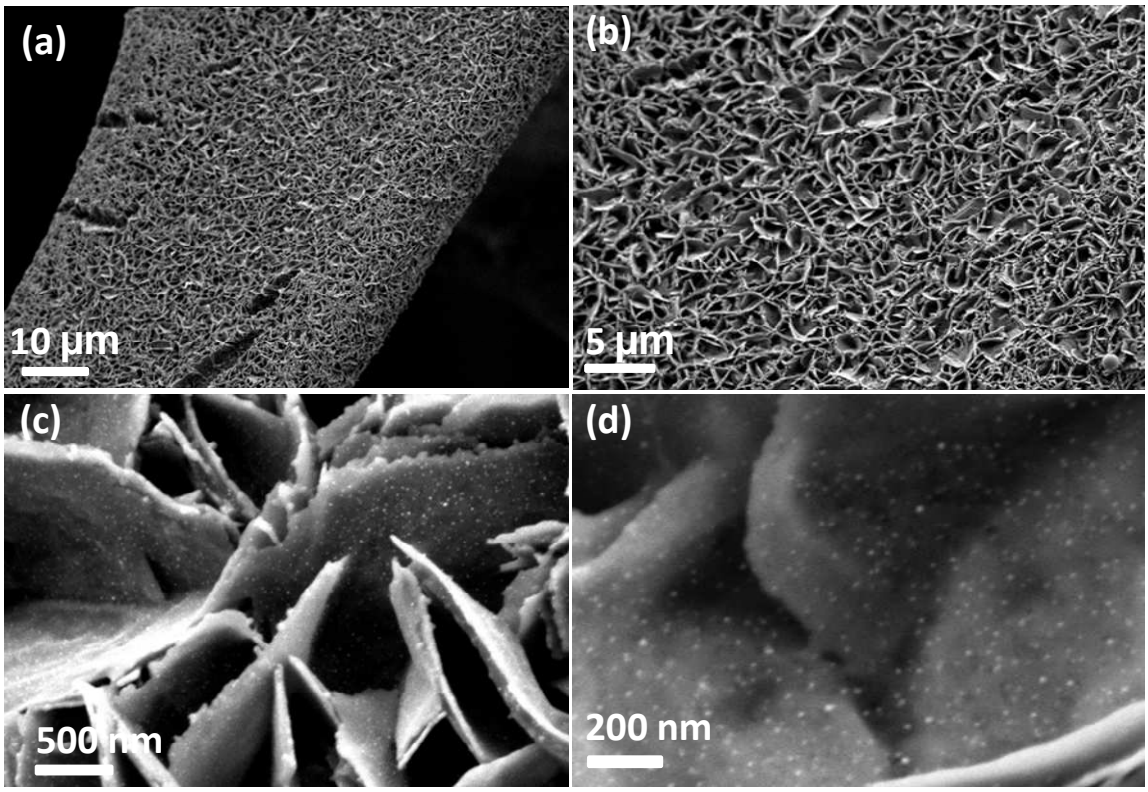

Fig. 3

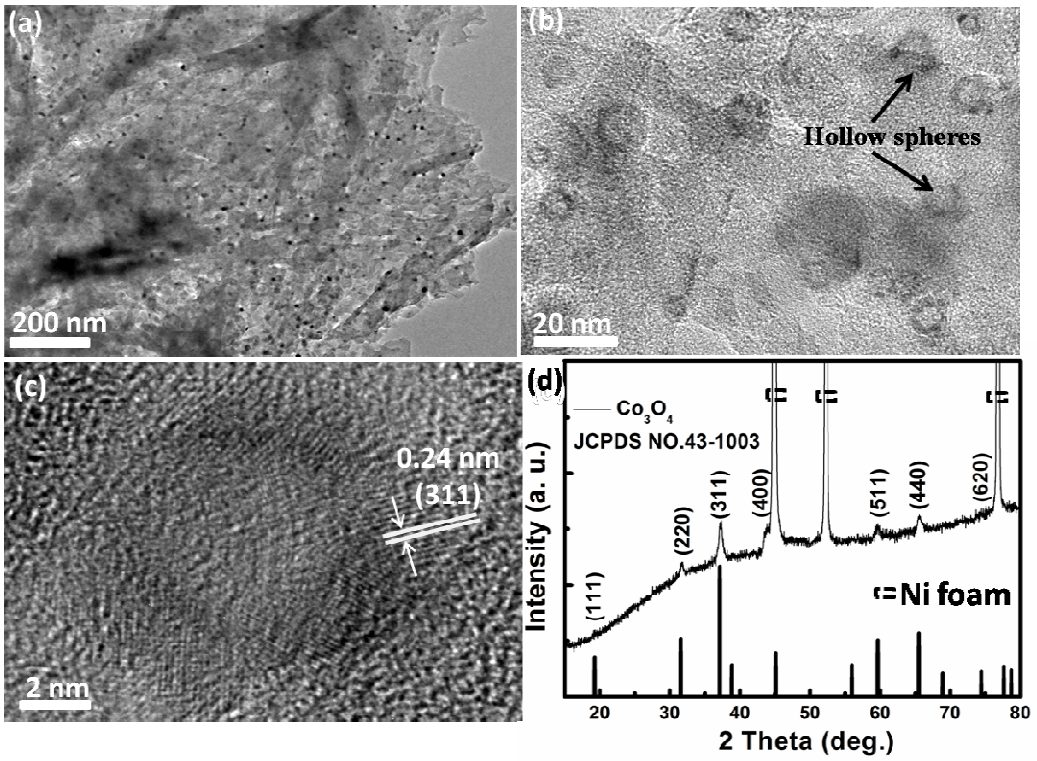

Fig. 4

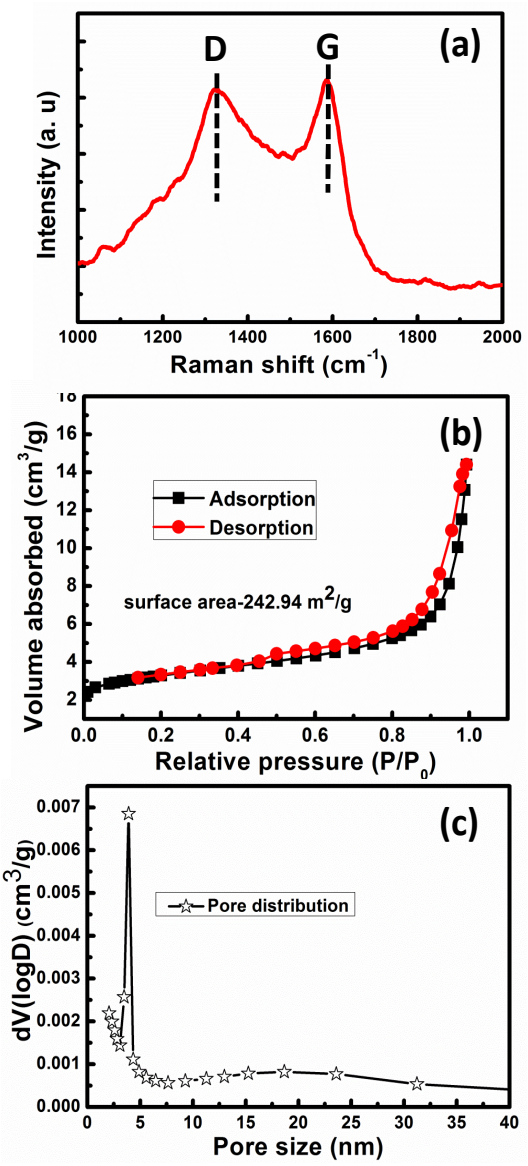

Fig. 5